

RMPs for Safe Impedance Control in Contact-Rich Manipulation

Seiji Shaw, Ben Abbatematteo, and George Konidaris
 {sshaw4, babbatem, gdk}@cs.brown.edu

Abstract— Variable impedance control in operation-space is a promising approach to learning contact-rich manipulation behaviors. One of the main challenges with this approach is producing a manipulation behavior that ensures the safety of the arm and the environment. Such behavior is typically implemented via a reward function that penalizes unsafe actions (e.g. obstacle collision, joint limit extension), but that approach is not always effective and does not result in behaviors that can be reused in slightly different environments. We show how to combine Riemannian Motion Policies, a class of policies that dynamically generate motion in the presence of safety and collision constraints, with variable impedance operation-space control to learn safer contact-rich manipulation behaviors.

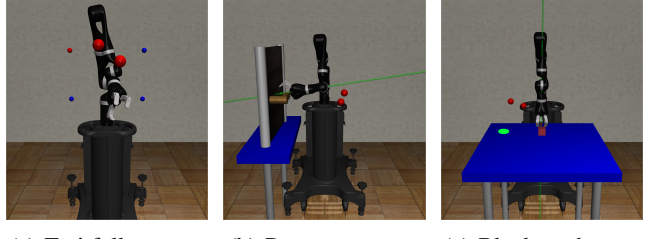
I. INTRODUCTION

Learning autonomous contact-rich manipulation behavior is a critical challenge for robotics; indeed, the very purpose of a robot is often to make contact with the environment in order to manipulate it. However, contact-rich behavior is challenging—robots must be able to reason about sudden constraints when contacting target objects and model the unknown dynamics of the objects they are manipulating.

To address these issues, Martin-Martin et al. [1] discuss the advantages of formulating the task in the robot’s end-effector space. They propose the use of variable impedance control in end-effector space (VICES), which defines the robot’s next actions in terms of displacements and compliance of the end-effector. The VICES commands are then translated back as lower-level torque commands to the joints in the arm by an operational-space impedance controller (OSC). When training an agent using reinforcement learning, the policy is trained to output actions in the VICES action-space, directly controlling end-effector behavior, and can manage the discontinuous mode-changes made at contact using the compliance component of the space.

While the VICES modality serves as a useful layer of abstraction for learning and transfer, the agent loses the ability to reason about the configuration of the rest of its arm in relation to the environment. This can lead to routine hyperextension and collisions during and after training, which are undesirable and potentially dangerous. The problem of safe variable impedance control has therefore not yet been solved robustly [2].

We present RMP-VICES, a controller that accounts for the geometry of the arm and its surrounding environment by generating motor torques that drive the arm to avoid joint limits and obstacles. We leverage Riemannian motion policies (RMPs), which allow a user to specify different behaviors



(a) Traj-follow. env. (b) Door-open. env. (c) Block-push. env.

Fig. 1: Instances of task environments with randomly-generated obstacles (red spheres).

in more convenient ‘task’ manifolds and then synthesize them [3], [4]. Most importantly, RMPs have a mechanism (the Riemannian metric of these task spaces/manifolds) for designating the priority of these behaviors, which can vary based on the current position and velocity of the arm. We reformulate VICES impedance controller as an attraction-type Riemannian motion policy, and synthesize it with obstacle repulsion behavior and a joint limit controller [4]. We then use the RMP-Tree to translate VICES outputs into motor-torques that allow the robot to safely move through the environment. We verify the efficacy of our approach by training a 7DOF Kinova Jaco 2 on three different simulated domains and analyzing the frequency and severity of collision and joint limit events that occur over the course of learning. Afterwards, we run the trained agents in the same domains with randomly-placed obstacles to evaluate RMP-VICES’s ability to adapt to obstacles not present in training. RMP-VICES reduces the number of collision by up to 50% and joint limit events by up to 90% in all of these domains.

II. BACKGROUND

A. Reinforcement Learning

A Markov Decision process \mathcal{M} is given by a tuple $(\mathcal{S}, \mathcal{A}, \mathcal{R}, \mathcal{T}, \gamma)$. An agent receives scalar reward r_t for taking action $a \in \mathcal{A}$ in state $s \in \mathcal{S}$ according to $\mathcal{R}(s, a)$. The state evolves according to the transition function $\mathcal{T}(s, a)$; in our setting \mathcal{S} and \mathcal{A} are continuous spaces. The goal of reinforcement learning is to find a policy π which maximizes the expected discounted return

$$\max_{\theta} \mathbb{E}_{\mathcal{M}, \pi} \left[\sum_t \gamma^t r_t \right], \quad (1)$$

where γ is a discount factor. Policy search methods are a family of algorithms that search directly over a space of parameterized policies. In practice, the class of parameterized

policies is typically chosen such that it can represent an expressive family of robot motions while supporting important properties such as stability.

B. Variable Impedance Control in End-Effector Space

VICES enables agents to use end-effector space (SE(3)) and compliance of the end-effector as the action space of the agent. More formally, VICES defines an action $a = (\Delta p, k_{pos}^p, k_{ori}^p) \in \mathcal{A} = \text{SE}(3) \times \mathbb{R}^3 \times \mathbb{R}^3$, where k_{pos}^p and k_{ori}^p are vector representations of stiffness matrices in an impedance controller.

In a single timestep, Δp is composed with the current end-effector position to produce desired setpoints p_{des} and R_{des} . We then compute the corresponding joint torques using Khatib's formulation of operation space control [5], [6]:

$$u = J_{pos}^T [\Lambda^{pos} [k_{pos}^p (p_{des} - p) - k_v^{pos} v]] + J_{ori}^T [\Lambda^{ori} [e_r (R_{des}, R) - k_v^{ori} \omega]], \quad (2)$$

where J_{pos} and J_{ori} are the Jacobians associated with the forward-kinematics map to end-effector position p and orientation R , Λ^{pos} and Λ^{ori} the corresponding end-effector inertia matrices, and v and ω the velocity and angular velocity of the end-effector. We compute damping matrices k_v^{pos} and k_v^{ori} so that the system is critically damped relative to given k_{pos}^p and k_{ori}^p as chosen by the agent. e_r is an error on SO(3) that can be used for impedance controllers [7]; see section III-B.

The greatest strength and weakness of VICES is that the control signal (actions) u and states are restricted to the end-effector space, SE(3). While this means that the agent will learn policies that can be transferred from one robot to another using SE(3) as a layer of abstraction, the policy is not able to reason about its joint states (and by proxy, the pose of the robot's links) that lead to its end-effector configuration to avoid collision.

C. Riemannian Motion Policies

Riemannian motion policies (RMPs) are a mathematical framework that decomposes complex robot motion behavior into individual behaviors specified in more interpretable task spaces [3]. RMPs enable the controllers to be expressed in their appropriate task spaces and then manage the transforms and flow of control between those spaces to the robot's configuration space, which is where control must ultimately occur. Additionally, they allow us to blend multiple such controllers to, for example, reach to a point (an attractive controller between the robot's end-effector and a target location) while avoiding obstacles (a repulsive or dissipative controller between the robot's arm and obstacles in its 3D environment).

RMPs are organized in a tree-like structure—the RMP-Tree—where the root represents the robot's configuration manifold \mathcal{Q} , and every node represents a task manifold (e.g. SE(3)). The edges of the tree represent maps from the positions in the parent task space to the child task space (for an example, see 2). Here, we denote a parent space as \mathcal{M}

and the i th child space as \mathcal{N}_i . We will write the map from \mathcal{M} to \mathcal{N}_i will be written as ϕ_i .

Individual component behaviors to be synthesized are represented by maps from position and velocities to forces at the leaf nodes. If \mathcal{N} is a leaf task-space, we notate the behavior map as $f(x, \dot{x})$. The priority of each of these behaviors is specified by a positive-semidefinite tensor that resembles the Riemannian metric of these task manifolds, which can vary based upon the position and velocity in that task space. We denote this metric as $M(x, \dot{x}) \in \mathbb{R}^{n \times n}$, where $n = \dim \mathcal{N}$, and $x \in \mathcal{N}$.

RMP-trees are evaluated in two phases: pushforward and pullback. In pushforward, the current state of the arm (q, \dot{q}) is propagated through the tree to compute the state in each child manifold. In pullback, forces f_i are evaluated at each child manifold and then synthesized back to compute the joint accelerations \ddot{q} at that timestep.

1) *Pushforward*: Let \mathcal{M} be a parent space, and let \mathcal{N}_i be one of its child spaces, and let x, \dot{x} be a computed position and velocity in \mathcal{M} . In pushforward, the corresponding position y and velocity \dot{y} in \mathcal{N}_i are computed as follows:

$$y = \phi_i(x), \quad \dot{y} = J_{\phi_i} \dot{x},$$

where J_{ϕ_i} is the Jacobian of task-mapping ϕ_i .

2) *Pullback*: After pushforward is complete, we have position and velocity in each of the leaf task manifolds. We then must evaluate each policy f_i and propagate the force signal back to the configuration manifold. Given parent manifold \mathcal{M} and child leaf manifold \mathcal{N}_i , with position y and velocity \dot{y} in \mathcal{N}_i we first evaluate $\ddot{y} = f_i(y, \dot{y})$ to find the corresponding leaf's acceleration, and $M_i(y, \dot{y})$ to find the Riemannian-metric priority tensor. We then compute the corresponding acceleration \ddot{x} and metric M in \mathcal{M} as follows:

$$\ddot{x} = \sum_{i=1}^n J_{\phi_i}^T (\ddot{y} - M_i(y, \dot{y}) J_{\phi_i} \dot{x}), \quad M = \sum_{i=1}^n J_{\phi_i}^T M_i(y, \dot{y}) J_{\phi_i}.$$

We then recursively pullback from the leaf nodes to the root node and find the joint accelerations by computing $\ddot{q} = M^{\dagger} f$, where M^{\dagger} is the Moore-Penrose pseudo-inverse of M . This process solves the least-squares problem that trades off policy outputs with respect to each metric M_i .

3) *Related Work on RMPs*: RMPs build on many earlier methods that decompose behavior into a number of different task spaces. Nakamura et al. [8], Sentis et al. [9], and Coelho and Grupen [10] all propose similar frameworks that decompose the robot task space in recursively-defined nullspaces. For each nullspace, an artificial potential field is used to define the movement. RMPs are formulated in such a way that subsume these methods. Furthermore, RMPs can have more than one behavior per space with appropriate Riemannian metric design, providing a richer set of tools to describe robot behavior.

RMPs have been used primarily to guide robot arms through free space in a variety of reaching and manipulation-based tasks [11], [12], [13], [14], [15]. However, none

of them perform contact-rich manipulation by training an agent whose actions are translated into attraction-type behavior in the RMP-tree itself. While not addressing contact-manipulation problems, Li et al. [11] introduces RMP², a framework that allows an agent to learn with RMPs to accomplish 2D reaching tasks safely using state-of-the-art deep RL methods.

D. Related Work on Safe End-Effector Variable Impedance Control

An alternative approach to RMPs is to compute safety sets, and ensure that the policy stays within those bounds. Wabersich and Zeilinger [16] propose a general formulation of a learning problem where these bounds can be computed. Once the safety set is known, a method such as control barrier functions [17], [18] can be used to ensure that the policy stays within that set (termed *forward set-invariance*). However, finding these safety sets are computationally expensive, while RMPs can be constructed from known obstacle pose data at runtime without any prior computing other than setting up the tree. While these methods are compelling due to their formal safety guarantees, we have yet to see them applied for safety of an impedance-control scheme in learning to solve contact-rich manipulation tasks.

Many have discussed formulations of impedance control to ensure Lyapunov stability. Khader et al. [19] constrain the stiffness parameters of the action space to ensure that their controller is Lyapunov-stable, and thus resilient to perturbations and unexpected behavior. Others prove Lyapunov-stability for more general formulations of learning problems [20], [21]. Lyapunov-stability guarantees a convergence property of the system showing that the system state must be contained in smaller regions of the space as dynamics evolve in accordance to the Lyapunov function. However, since Lyapunov-stability discusses *convergence* and not *safety-set forward-invariance*, these methods are not evaluated for safety using the same metrics used here.

III. RMP-VICES

A naive operational-space controller (e.g. as in VICES [6]) fails to reason about collision with the environment and violation of the arm's joint limits. We propose RMP-VICES, an operational-space controller which translates SE(3) impedance commands from a learned policy to low level torques that accounts for the geometry of the configuration space and surrounding environment. We formalize variable-impedance control as an attractor-type RMP, and fuse it with repulsion-type RMPs based at points sampled from the robot's arm. The resulting controller blends the desired policy control with collision avoidance behavior in training and in deployment.

A. Tree Structure

The forward-kinematics map to the last link of the arm is used to compute the pose of the end-effector in SE(3). We then perform a selection mapping to decompose SE(3) into \mathbb{R}^3 and SO(3), and define the variable impedance behavior

in those spaces. We perform an identity map from the robot's configuration space to itself, where define the joint-limiting behavior as shown in Cheng et al. [4].

For the purpose of collision avoidance, we sample control points on the links of the arm, and define distance spaces to each obstacle. Since we conducted training with a 7DOF arm, we need seven different forward kinematics maps from the configuration space to SE(3) for the pose of each individual link of the arm. From each of the sampled control points, we compute a selection map to \mathbb{R}^3 and then a distance map to \mathbb{R} for each obstacle, and define collision-avoidance behavior there. A schematic of the RMP-tree can be seen in Fig. 2.

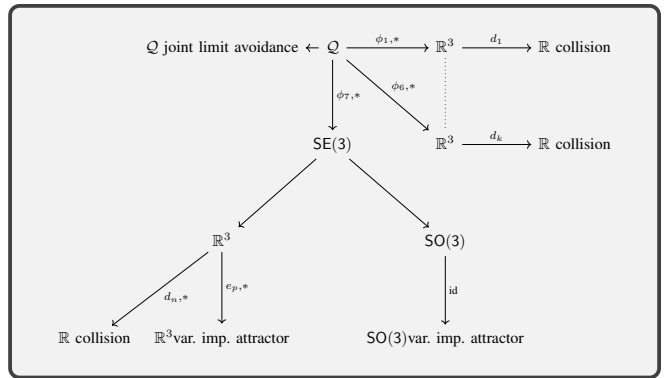


Fig. 2: The RMP-tree structure used for RMP-VICES. $\phi_1, \phi_2, \dots, \phi_7$ denote forward-kinematics maps from \mathcal{Q} to each link of the arm, where the variable impedance behavior sits in SE(3). The rest of the RMP-tree is made up to control points sampled from the link meshes, which are mapped to the shortest-distance space each obstacle (d_1, \dots, d_n act as signed-distance functions) where collision avoidance is defined. The selection map from SE(3) to \mathbb{R}^3 has been omitted.

B. Impedance Control as Attractor-type RMPs

We formulate impedance controllers as RMP leaves in the \mathbb{R}^3 and SO(3) task spaces. Both of these controllers are formulated as attraction-type policies [3].

Let $x \in \mathbb{R}^3$ be a position of the end-effector in free space and \dot{x} be its associated velocity as computed by the pushforward operation. Let $x_g \in \mathbb{R}^3$ be a desired position. Then the motion behavior is formulated as a spring-damper attractor-type policy in \mathbb{R}^3 :

$$f(x, \dot{x}) = k_p(x - x_g) - k_d(\dot{x}), \quad (3)$$

with the associated metric being the identity matrix I . The diagonal matrices k_p^{pos} and k_d^{pos} specify the stiffness of this controller and are set by the trained policy at every timestep.

The attractor in SO(3) is written in a very similar way to the RMP above, except we also must account for the non-Euclidean topology of SO(3) in the error term. Let $r \in SO(3)$ and ω be the end-effector's current orientation and angular velocity, and r_g be the desired orientation. We

represent $r = [r_x, r_y, r_z]$ and $r_g = [r_{gx}, r_{gy}, r_{gz}]$ as rotation matrices, i.e.

We then use the same error term on $\text{SO}(3)$ from VICES:

$$e_r(r, r_g) = \frac{1}{2} (r_x \times r_{xg} + r_y \times r_{yg} + r_z \times r_{zg}). \quad (4)$$

This error is equivalent to the sine of the angle to rotate r to r_g about a single axis [7]. We then define the impedance controller using this error:

$$f(r, \omega) = k_p^{ori} \cdot e_r(r, r_g) - k_d^{ori} \cdot \omega, \quad (5)$$

where k_p , k_d are the stiffness and damping coefficients respectively. As before, the metric associated with this attraction-type policy is the identity I .

It is important to note that removing the obstacle-avoidance and joint-limit policies from the RMP-tree reduces the controller to VICES [3], [1].

C. Collision Avoidance RMPs

For both types of obstacles, we use the signed-distance function to map the position of the control point sampled on the arm to the distance space between the point and the obstacle. We define the Riemannian metric $m(x, \dot{x}) \in \mathbb{R}$ of this 1-dimensional space to be the following expression:

$$m(x, \dot{x}) = \begin{cases} \frac{\dot{x}^2}{x^4}, & \dot{x} > 0 \\ 0, & x \leq 0. \end{cases} \quad (6)$$

As described in [3], the collision policy will only activate and strengthen if the control point is moving towards the obstacle. For both planar and spherical collision-avoidance behaviors, we do not provide a repulsive signal but a damping term ($f(x, \dot{x}) = \eta \dot{x}$, for some damping coefficient η). As Bylard et al. in [22] observe, using only the Riemannian metric and a dissipation function to reduce the movement towards the obstacle to generate collision-avoidance behavior reduces the likelihood of the arm to trap itself in local-minima.

D. Integrating Policy Actions in the RMP-VICES Controller

In an MDP formulation of a manipulation task, our state space will always be a superset of $\text{SE}(3) \times S_{obj}$, where $\text{SE}(3)$ is the spaces of end-effector pose and S_{obj} is the space of states of the manipulated object. An action will be a tuple $(\Delta x, k_p^{pos}, k_p^{ori}) \in \text{SE}(3) \times \mathbb{R}^3 \times \mathbb{R}^3$, where Δx is a displacement in $\text{SE}(3)$ for the next goal pose and k_p^{pos} and k_p^{ori} are the stiffness coefficients for the impedance controllers (k_d is computed so the impedance controllers are critically-damped). The policy π will be sampled in pushforward and used to update k_p^{pos} , k_p^{ori} , k_d^{pos} , k_d^{ori} , and r_g , and x_g in eqs. 3 and 5 in the RMP-tree on every timestep.

After the pullback stage of the RMP, we obtain a corresponding joint acceleration \ddot{q} given by the synthesis of the end-effector impedance control and collision avoidance behavior. To convert \ddot{q} into joint torques, we multiply by the inertia matrix of the arm in joint space and compensate for gravity and Coriolis forces.

IV. EXPERIMENTS

We test and verify the efficacy of RMP-VICES on the trajectory-following and door-opening domains constructed in Martin-Martin et al. [1] and an additional block pushing domain we developed. In each simulated domain, we first train VICES and RMP-VICES in an environment with no additional obstacles to evaluate any negative impact the RMP-tree has on learning efficiency. We also record the force of all collisions of the arm with objects in the workspace to understand the severity of collisions events using VICES and RMP-VICES. Collision and joint-limit events incur a penalty in the reward function and termination of the episode (but an ablation on these two properties showed that they were not essential for effective training). Afterwards, we perform 100 rollouts with the learned policy in each domain with two randomly placed spherical obstacles and record the force of any collision-events to verify the adaptability of each algorithm to obstructions not seen during training.

All simulated experiments were conducted in Robosuite [23]. The agent was given a stochastic policy parameterized by two fully-connected layers of 64 nodes with tanh activations and optimized using PPO, as done in VICES. Our PPO implementation is based on the code written for OpenAI's SpinningUp [24]. In each domain, each episode was given a length of 1024 steps, with 4096 steps per epoch. The policy network was initialized with random weights (10 seeds) and was trained for 367 epochs (1.6×10^6 training steps).

A. Environments

1) *Trajectory-Following*: We randomly place four via points in the workspace, and specify an order in which the robot end-effector must traverse through them. As in VICES, the state of the agent is represented by the pose and the velocity of the end-effector, the position of each via-point, and whether each via-point has been checked. For the rollouts after training, we randomly generated two spherical obstacles with a radius of 5 cm in the bounding volume that is used to generate the via-points. We ensured that no obstacles overlapped with a via-point so that the task still had a guaranteed solution.

2) *Door-Opening*: The RMP-tree was initialized with two plane collision avoidance policies to avoid the panel of the door and the surface of the table. For the rollouts after training, we generate two spherical obstacles in a bounding volume placed at a distance of front of the door to ensure that it can still swing open for task completion.

3) *Block-Pushing*: We constructed a novel domain where the robot must push a block across a table to a goal position. The state includes the end-effector's pose and distance to the block as well as the distance between the block and the goal position. The reward function gives a small shaped reward that depends on the distance between the end-effector and the goal, and a larger shaped reward between the cube and the goal:

$$r_{main}(d_{h2c}, d_{c2g}) = r_{h2c} * (1 - \tanh(20d_{h2c})) + r_{c2g} * (1 - \tanh(20d_{c2g})), \quad (7)$$

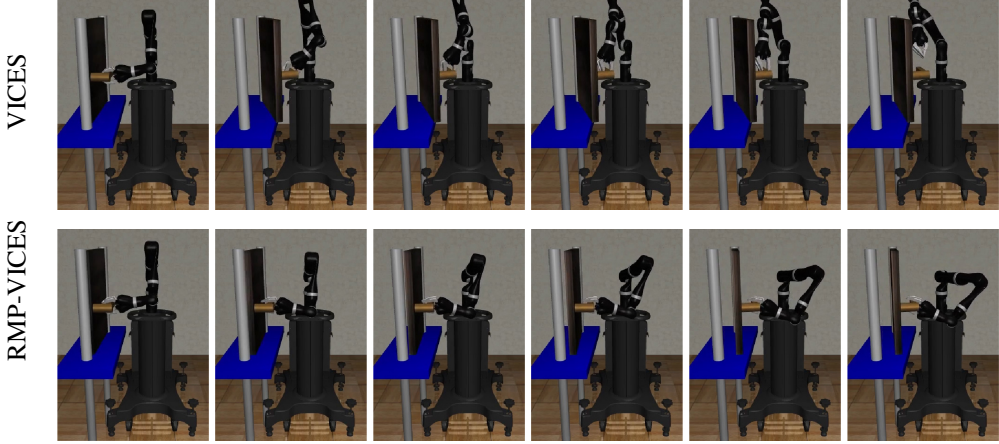


Fig. 3: Regularly-timed stills of a single rollout of VICES (top) and RMP-VICES (bottom) after training is complete.

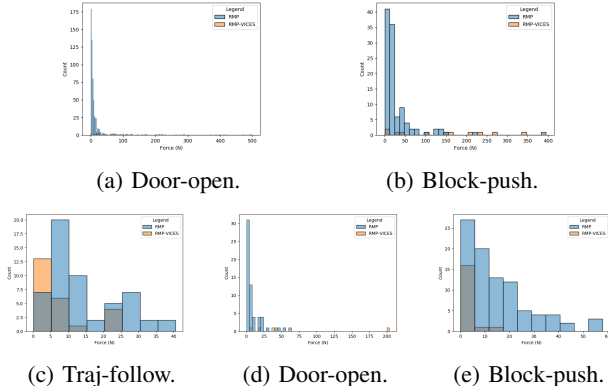


Fig. 4: Severity of collision events in training (a,b), and in environments with randomly generated obstacles (c-e).

where d_{h2c} , d_{c2g} are the distance from the hand to the cube, and distance from the cube to the goal separately. r_{h2c} and r_{c2g} are the maximum rewards made to provide incentive for the agent to bring the end-effector to the cube, and the cube to the goal, respectively.

V. RESULTS

A. Safety During Training

In the trajectory-following task, RMP-VICES has far fewer joint-limit events than VICES (fig. 5b) throughout training. Furthermore, RMP-VICES learns more sample-efficiently than just VICES alone (fig. 5a). Since joint limiting behavior causes episode termination, RMP-VICES has access to more viable data earlier in training, which accelerates the agent’s ability to learn the task.

In the door-opening task, we see that while RMP-VICES avoids collision better than VICES (figs. 5e, 4a), the agent trained with RMP-VICES learns with worse overall performance (fig. 5d). However, RMP-VICES is significantly safer in guiding the robot away from collision avoidance behavior, which ultimately is more important than the degree to which the robot succeeds at its given task. After reviewing several

rollouts of each policy (fig. 3), we see that the VICES-trained policy learns a behavior that keeps the robot’s pose largely the same with the arm elbow pointing straight up, which the RMP-VICES joint-limit and collision-avoidance policy represses. As a result, the RMP-VICES policy first pitches the elbow downward, and then opens the door. Since we give a dense reward that increases with door angle, the RMP-VICES agent obtained a lower average reward in VICES. However, the RMP-VICES policy is a safer behavior than the one learned by VICES alone, since the VICES behavior is prone to collision with the door (fig. 3).

In the block-pushing task, we see that RMP-VICES starts with better joint-limiting performance at the beginning of training figs. 5h 5i. While VICES performs slightly better than RMP-VICES in efficacy of learning, RMP-VICES is much more performant in collision avoidance throughout training.

B. Deployment in Environments with Generated Obstacles

For each experiment, we choose the best performing seeds from the VICES-trained and RMP-VICES trained agent from each domain, and played through 100 episodes with randomly-generated spherical obstacles in the environment. The size and location of the bounding volumes used for each domain were chosen as areas where the arm would frequently pass through to the solve the task. Table I gives an aggregation of the performance of VICES and RMP-VICES from this set of experiments. See fig. 1 in the supplementary materials for visualizations of all three environments for a single rollout instance.

Relative to performance in training, we see a drop in performance in all tasks. Intuitively, this makes sense, since neither the RMP nor RMP-VICES policies experienced these obstacles before training. We see from here that RMP-VICES, in all tasks, collides less frequently than VICES. While we do see a slight drop in performance in average reward, it is important to note that the success of the agent must be measured by its efficacy to complete the task *and* its ability to remain safe at the same time.

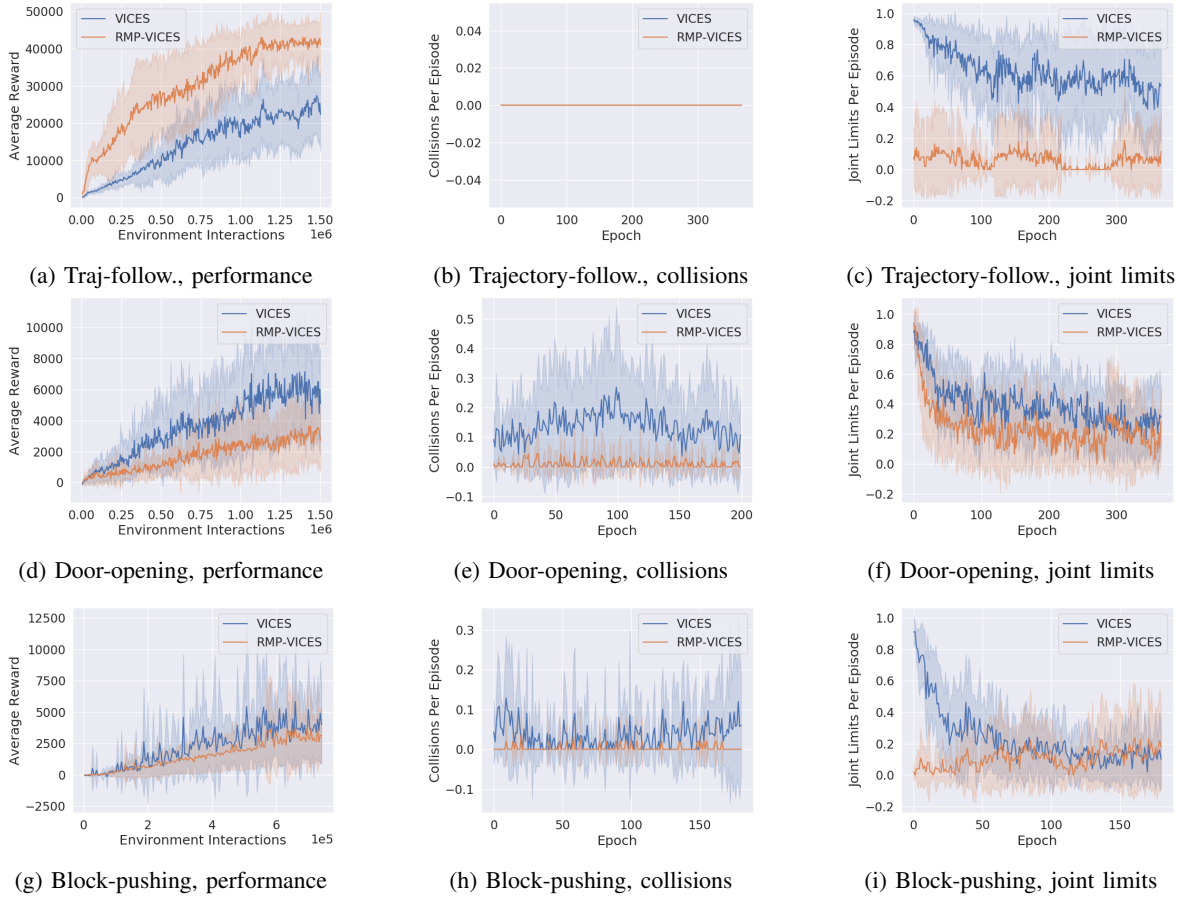


Fig. 5: Average reward, collision, and joint limit performance of VICES and RMP-VICES over the course of training on the trajectory-following (5a,5b,5c), door-opening (5d,5e,5f), and block-pushing domains (5d,5e,5f). When integrating the average curves for joint limits and collision avoidance behaviors, we see that RMP-VICES outperforms VICES in every domain. Percent decrease in collision and joint limit rates, respectively: trajectory-following: N/A%, 90.5%; door-opening: 39.8%, 90.7%; block-pushing: 54.6%, 93.2%.

	Task	Avg. Reward	Coll.	Joint Lim.
VICES	Traj-follow.	$7864 \pm 1.167 \times 10^4$	56	44
	Door-open.	$1703 \pm 1.948 \times 10^3$	61	36
	Block-push.	$1755 \pm 2.256 \times 10^3$	93	0
RMP-VICES	Traj-follow.	$6847 \pm 3.723 \times 10^3$	25	22
	Door-open.	$1051 \pm 6.96 \times 10^2$	5	11
	Block-push.	$1740. \pm 8.54 \times 10^2$	19	0

TABLE I: Results from rollouts in environments with randomly-generated obstacles. As in training, colliding with the environment or passing a joint limit triggers the episode to end, so the maximum number of collision and joint events for a single domain for a single agent is 100.

It is clear that the agent trained on RMP-VICES exploits the geometric prior given by the collision-avoidance RMPs for more safe behavior. An agent trained with VICES alone has no obvious way to incorporate this information, and the arm moves through the space blindly without adjusting its trajectory to avoid the new obstacles in its path.

Furthermore, we see that RMP-VICES reduces the impact

of collision between the arm and its surrounding environment. Here, we see that RMP-VICES in these domains exhibits a sharper distribution about 0N (fig. 4).

VI. CONCLUSION

We have presented RMP-VICES, a geometry-aware operational-space controller for contact-rich manipulation. Our formulation synthesizes learned impedance control in $SE(3)$ with predefined collision and joint limit avoidance behaviors, yielding a safer framework for reinforcement learning of manipulation skills. Our evaluation shows reduced frequency of collision and joint limit violation on the majority of tasks studied, especially early in learning. Future work is warranted to further investigate the design of safety behaviors and their interaction with policy optimization to maintain their effectiveness throughout the learning process and deployment.

REFERENCES

[1] R. Martín-Martín, M. A. Lee, R. Gardner, S. Savarese, J. Bohg, and A. Garg, “Variable impedance control in end-effector space: An action space for reinforcement learning in contact-rich tasks,” in 2019

IEEE/RSJ International Conference on Intelligent Robots and Systems (IROS), 2019, pp. 1010–1017.

[2] F. J. Abu-Dakka and M. Saveriano, “Variable impedance control and learning—a review,” *Frontiers in Robotics and AI*, vol. 7, p. 177, 2020. [Online]. Available: <https://www.frontiersin.org/article/10.3389/frobt.2020.590681>

[3] N. D. Ratliff, J. Issac, D. Kappler, S. Birchfield, and D. Fox, “Riemannian Motion Policies,” *arXiv e-prints*, p. arXiv:1801.02854, Jan. 2018.

[4] C.-A. Cheng, M. Mukadam, J. Issac, S. Birchfield, D. Fox, B. Boots, and N. Ratliff, “RMPflow: A Computational Graph for Automatic Motion Policy Generation,” *arXiv e-prints*, p. arXiv:1811.07049, Nov. 2018.

[5] O. Khatib, “Inertial properties in robotic manipulation: An object-level framework,” *International Journal of Robotics Research*, vol. 14, p. pp., 1995.

[6] —, “A unified approach for motion and force control of robot manipulators: The operational space formulation,” *IEEE Journal on Robotics and Automation*, vol. 3, no. 1, pp. 43–53, 1987.

[7] J. Luh, M. Walker, and R. Paul, “Resolved-acceleration control of mechanical manipulators,” *IEEE Transactions on Automatic Control*, vol. 25, no. 3, pp. 468–474, 1980.

[8] Y. Nakamura, H. Hanafusa, and T. Yoshikawa, “Task-priority based redundancy control of robot manipulators,” *The International Journal of Robotics Research*, vol. 6, no. 2, pp. 3–15, 1987. [Online]. Available: <https://doi.org/10.1177/027836498700600201>

[9] L. Sentis and O. Khatib, “Synthesis of whole-body behaviors through hierarchical control of behavioral primitives,” *International Journal of Humanoid Robotics*, vol. 2, no. 04, pp. 505–518, 2005.

[10] J. A. Coelho Jr and R. A. Grupen, “A control basis for learning multifingered grasps,” *Journal of Robotic Systems*, vol. 14, no. 7, pp. 545–557, 1997.

[11] A. Li, C.-A. Cheng, M. A. Rana, M. Xie, K. Van Wyk, N. Ratliff, and B. Boots, “RMP2: A Structured Composable Policy Class for Robot Learning,” in *Robotics: Science and Systems (R:SS)*, 2021.

[12] M. Mukadam, C.-A. Cheng, D. Fox, B. Boots, and N. Ratliff, “Riemannian Motion Policy Fusion through Learnable Lyapunov Function Reshaping,” *arXiv e-prints*, p. arXiv:1910.02646, Oct. 2019.

[13] M. A. Lee, C. Florensa, J. Tremblay, N. Ratliff, A. Garg, F. Ramos, and D. Fox, “Guided Uncertainty-Aware Policy Optimization: Combining Learning and Model-Based Strategies for Sample-Efficient Policy Learning,” *arXiv e-prints*, p. arXiv:2005.10872, May 2020.

[14] A. Handa, K. Van Wyk, W. Yang, J. Liang, Y. W. Chao, Q. Wan, S. Birchfield, N. Ratliff, and D. Fox, “Dexpilot: Vision-based tele-operation of dexterous robotic hand-arm system,” in *2020 IEEE International Conference on Robotics and Automation (ICRA)*, 2020, pp. 9164–9170.

[15] D. Kappler, F. Meier, J. Issac, J. Mainprice, C. G. Cifuentes, M. Wüthrich, V. Berenz, S. Schaal, N. Ratliff, and J. Bohg, “Real-time perception meets reactive motion generation,” *IEEE Robotics and Automation Letters*, vol. 3, no. 3, pp. 1864–1871, 2018.

[16] K. P. Wabersich and M. N. Zeilinger, “Linear model predictive safety certification for learning-based control,” in *2018 IEEE Conference on Decision and Control (CDC)*, 2018, pp. 7130–7135.

[17] T. Wei and C. Liu, “Safe control algorithms using energy functions: A unified framework, benchmark, and new directions,” in *2019 IEEE 58th Conference on Decision and Control (CDC)*, 2019, pp. 238–243.

[18] R. Cheng, G. Orosz, R. M. Murray, and J. W. Burdick, “End-to-end safe reinforcement learning through barrier functions for safety-critical continuous control tasks,” *Proceedings of the AAAI Conference on Artificial Intelligence*, vol. 33, no. 01, pp. 3387–3395, Jul. 2019. [Online]. Available: <https://ojs.aaai.org/index.php/AAAI/article/view/4213>

[19] S. A. Khader, H. Yin, P. Falco, and D. Kragic, “Stability-guaranteed reinforcement learning for contact-rich manipulation,” *IEEE Robotics and Automation Letters*, vol. 6, no. 1, pp. 1–8, 2021.

[20] Y. Chow, O. Nachum, E. Duenez-Guzman, and M. Ghavamzadeh, “A lyapunov-based approach to safe reinforcement learning,” *arXiv preprint arXiv:1805.07708*, 2018.

[21] F. Berkenkamp, M. Turchetta, A. Schoellig, and A. Krause, “Safe model-based reinforcement learning with stability guarantees,” in *Advances in Neural Information Processing Systems*, I. Guyon, U. V. Luxburg, S. Bengio, H. Wallach, R. Fergus, S. Vishwanathan, and R. Garnett, Eds., vol. 30. Curran Associates, Inc., 2017.

[22] A. Bylard, R. Bonalli, and M. Pavone, “Composable Geometric Motion Policies using Multi-Task Pullback Bundle Dynamical Systems,” *arXiv e-prints*, p. arXiv:2101.01297, Jan. 2021.

[23] Y. Zhu, J. Wong, A. Mandlekar, and R. Martín-Martín, “robosuite: A modular simulation framework and benchmark for robot learning,” in *arXiv preprint arXiv:2009.12293*, 2020.

[24] J. Achiam, “Spinning Up in Deep Reinforcement Learning,” 2018.